Springer

KSME

Journal of Mechanical Science and Technology 28 (7) (2014) 2879~2888

www.springerlink.com/content/1738-494x
DOI 10.1007/s12206-014-0641-1

Trajectory planning for overhead crane by trolley acceleration shaping †

Nguyen Quang Hoang[1], Soon-Geul Lee[2,*], Hyung Kim[2] and Sang-Chan Moon[2]

[1]*Hanoi University of Science and Technology, No. 1 Dai Co Viet Road, Hanoi, Vietnam*
[2]*Kyung Hee University, 1732 Deokyoungdae-ro, Giheung-gu, Yongin, Gyeonggi-do, 446-701, Korea*

(Manuscript Received October 6, 2013; Revised February 18, 2014; Accepted February 26, 2014)

Abstract

This paper proposes a novel off-line trolley trajectory planning method for underactuated overhead cranes. The proposed technique is feasible and efficient for overhead crane operation. Dynamic coupling between trolley motion and payload swing was successfully exploited using a staircase form of trolley acceleration. The payload swings in the constant velocity phase were efficiently suppressed and the trolley reached the desired position using this technique. The reasonable number of stairs can be determined by evaluating the residual oscillation amplitude according to the number of stairs and variation in the natural frequency of the pendulum. The proposed approach was first simulated from the kinematics viewpoint to verify the validity of the trolley trajectory and the swing angle of the payload. The proposed approach was then combined with the dynamics of the overall crane, wherein the robust sliding mode controller was applied to ensure that the trolley tracks the designed trajectory. The numerical simulation results demonstrated superior performance and robustness against parameter uncertainties of the proposed method. The proposed method exhibited potential for application in the control of underactuated systems, such as overhead cranes, single-link flexible-joint manipulators, and flexible Cartesian manipulators.

Keywords: Underactuated system; Overhead cranes; Anti-swing trajectory planning; Acceleration shaping

1. Introduction

Overhead cranes are widely used in various fields, such as heavy industries, seaports, automotive factories, and construction facilities. The productivity and efficiency of an overhead crane depends on payload weight and velocity, as well as on the capability of the crane to quickly reduce the swing angle of the payload after each operation. Theory and practice have shown that high acceleration and deceleration correspond to large swing angles. This condition leads to hazardous situation and may cause serious accidents when the cargo swing angle becomes extremely large. A large cargo swing angle can break the crane, damage other equipment and infrastructure, or harm nearby people.

The process of operating a crane can be divided into three phases, namely, payload lifting, horizontal transportation, and payload lowering. The second phase presents the most difficult challenge. For this phase, the trolley and the payload need to quickly reach the desired position. Meanwhile, the swing angle of the payload must remain small and must return to zero at the end of each operation. Two main approaches may be applied to satisfy this requirement: the design of an anti-swing controller and the design of a reasonable trajectory for the trolley, otherwise known as motion planning. In the second approach, the desired trajectory normally comprises three phases, namely, acceleration, maintaining constant velocity, and deceleration. The time and shape of acceleration in the first and third phases are chosen such that the swing angle of the payload reaches the maximum, and then decreases to zero.

The first approach has drawn interest from various fields of study. A number of control algorithms have been developed for overhead cranes. The simplest approach is designing a linear controller based on the linearized model around its target location. This technique assumes a small payload swing during an operation. The crane dynamics can initially be a linearized model around its target location; subsequently, linear control approaches can be designed according to this model. This technique can be combined with optimal control and extended by gain scheduling [1] and input shaping [2-4].

To improve performance, various nonlinear and advanced control strategies have been tested on the crane control problem. These strategies include partial feedback linearization [5-9], sliding mode control [10-14], and adaptive control [5, 15-18]. A combination of the control methods has also been considered, such as adaptive sliding mode control [19-23] and adaptive fuzzy sliding mode control [24].

A design method based on the energy and passivity of the system has recently been investigated. This approach has been successfully applied in the control of underactuated systems

*Corresponding author. Tel.: +82 31 201 2506, Fax.: +82 31 202 1204
E-mail address: sglee@khu.ac.kr
† Recommended by Editor Jong Hyeon Park

such as overhead cranes [11, 15, 16, 25]. A controller that includes the passivity of the payload swing by using the payload as an end effector of a manipulator has been developed. H. Aschemann [26] applied energy shaping by interconnection and damping assignment according to a linearized model to increase the damping factor related to the underactuated coordinate.

Most controllers are designed for position regulation. These controllers may be difficult to implement when the trolley must travel over a large distance because of the limitation of the actuating force. Another problem is that these controllers require a sensor to measure trolley motion and another to measure the swing angle for feedback. This requirement increases the cost of the crane and may be difficult to implement.

In the second approach, the swing of the payload is suppressed by designing a reasonable trajectory for the trolley. This technique has also been evaluated. N. Sun et al. [15] applied iterative learning to determine the reasonable trajectory. However, the planned trajectory was obtained numerically. This iterative process needs to be repeatedly performed for each crane operation. H.-H. Lee [27] and N. Sun et al. [16] applied rectangular acceleration profile modifications to eliminate residual oscillations of a payload in the constant or zero velocity phase. Lee [28] used the acceleration in the sine form for the trolley in accelerating and decelerating phases. However, these methods require a precise natural frequency of the payload, which is dependent on the cable length. Thus, this technique is dependent on system parameters. N. Sun et al. [15] used an analytical function to generate an S-shaped trajectory for the trolley and obtain a smooth function for velocity and acceleration. However, with this function, the trolley can only reach its desired location when time approaches infinity.

This paper presents a novel trajectory planning method for overhead cranes, wherein the acceleration in a staircase form is used to eliminate the residual oscillation of the payload in the constant velocity phase and when the trolley reaches its desired location. The constraints on the acceleration amplitudes are given by a set of linear equations that can be easily evaluated. Numerical simulation results have demonstrated the efficiency of the proposed trajectory planning method. In addition, the planned trajectory is tracked by a simple robust controller that requires only the trolley motion for feedback. These findings suggest that the proposed scheme is efficient and feasible for crane control.

In summary, this paper has the following merits:

(1) The payload swing is theoretically proven to be zero during the constant velocity phase, and no residual swing exists when the trolley reaches the desired location.

(2) The trajectory planned by acceleration shaping is robust against uncertainties in the natural frequency of the payload, depending on the cable length.

(3) The residual vibration of the payload that depends on the number of stairs is investigated by simulation; this number of stairs should be three or five.

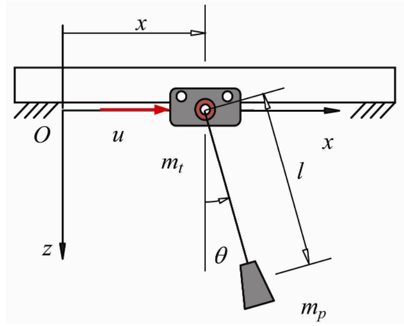

Fig. 1. 2D overhead crane model.

(4) An algorithm for trajectory planning is also presented; this is convenient for practical implementation because of its simple structure.

The remainder of this paper is organized as follows. Section 2 presents the problem formulation. Section 3 presents the method of acceleration shaping, wherein the trolley acceleration in a staircase form is applied to suppress the residual oscillation of the payload. Numerical experiments are demonstrated in Sec. 4. Finally, Section 5 concludes the paper.

2. Problem formulation

Trajectory planning for a crane during the horizontal transportation phase is presented in this paper. The rope has a constant length, and the system has two degrees of freedom. To obtain the dynamic model of the system, the following assumptions are established: (1) the payload is considered a point mass; (2) the mass and stiffness of the hoisting rope are disregarded; and (3) the effects of wind disturbances are disregarded. Based on the Lagrangian formulation [29], the dynamic model of a two-dimensional overhead crane system is expressed as follows:

$$(m_t + m_p)\ddot{x} + m_p l\cos\theta\,\ddot{\theta} - m_p l\dot{\theta}^2\sin\theta + f_{11}\dot{x} = u \tag{1}$$

$$m_p l\cos\theta\,\ddot{x} + m_p l^2\ddot{\theta} + m_p gl\sin\theta = 0 \tag{2}$$

where $x(t)$ denotes the trolley displacement, $\theta(t)$ denotes the payload swing angle (Fig. 1), and u is the force acting on the trolley. In this equation of motion, m_t and m_p represent the trolley mass and the payload mass, respectively; l is the length of the rope; g is the gravitational acceleration; and f_{11} is the damping coefficient on the trolley.

Crane dynamics consists of the actuated part described by Eq. (1) and the unactuated part described by Eq. (2). The second equation captures the kinematic coupling behavior between trolley acceleration $\ddot{x}(t)$ and the payload swing angle $\theta(t)$, which is given by

$$l\ddot{\theta} + g\sin\theta = -\cos\theta\,\ddot{x}. \tag{3}$$

In practice, the small swing angle of overhead cranes is usually maintained. Thus, the approximations for $\sin\theta \simeq \theta$ and $\cos\theta \simeq 1$ can be applied. Hence, Eq. (3) may be rewritten as

$$\ddot{\theta} + \omega_n^2\theta = -(\omega_n^2 / g)\,\ddot{x} \tag{4}$$

where $\omega_n = \sqrt{g/l}$ is the natural frequency of the payload modeled by the pendulum. Eq. (4) clearly shows that trolley acceleration directly influences payload swing. Therefore, a proper trajectory planning method for the trolley significantly affects the reduction or elimination of the payload swing.

Based on the practical operation of overhead cranes, some of the following requirements must be carefully considered through trajectory planning for the design specification of the trolley:

P1. The trolley reaches the target position within a finite time t_f; i.e.,

$$x(t) = p_d, \forall t \ge t_f . \tag{5}$$

P2. During movement, the trolley velocity and acceleration must be less than the maximum values

$$|\dot{x}_d(t)| \le v_{\max}, \qquad |\ddot{x}_d(t)| \le a_{\max} \tag{6}$$

where $v_{\max}$, $a_{\max}$ are the permitted maximum velocity and acceleration, respectively.

P3. The maximum payload swing must be kept within an acceptable domain,

$$|\theta(t)| \le \theta_{ub} . \tag{7}$$

P4. No swing should occur during the constant velocity phase, and when the trolley stops at the destination

$$\theta(t) = 0, \text{ when } \ddot{x}(t) = 0 \text{ and } \theta(t) = 0, \forall t \ge t_f . \tag{8}$$

Therefore, the trajectory $x(t)$ of the trolley must be designed such that the following conditions are satisfied:

$$\begin{aligned} &x(0) = 0,\ \dot{x}(0) = 0,\ \theta(0) = 0,\ \dot{\theta}(0) = 0 \\ &x(t_f) = p_d, \dot{x}(t_f) = 0, \theta(t_f) = 0, \dot{\theta}(t_f) = 0. \end{aligned} \tag{9}$$

3. Trajectory planning by trolley acceleration shaping

This section presents the design of a trolley trajectory that satisfies Eq. (9). This trajectory planning method is based on Eq. (2). If $\theta(t_0) = 0$, $\dot{\theta}(t_0) = 0$ and $\ddot{x}(t) = 0, t \ge t_0$ at time $t_0 \ge 0$, then the swing angle $\theta(t)$ becomes zero for all $t \ge t_0$, suggesting the design of the trolley trajectory with $\ddot{x}(t)$ in the accelerating $t \in [0, \tau_a]$ and decelerating phase $t \in [\tau_f - \tau_a, \tau_f]$ as

$$\begin{aligned} &\theta(\tau_a) = 0, \dot{\theta}(\tau_a) = 0 \\ &\theta(\tau_f) = 0, \dot{\theta}(\tau_f) = 0. \end{aligned} \tag{10}$$

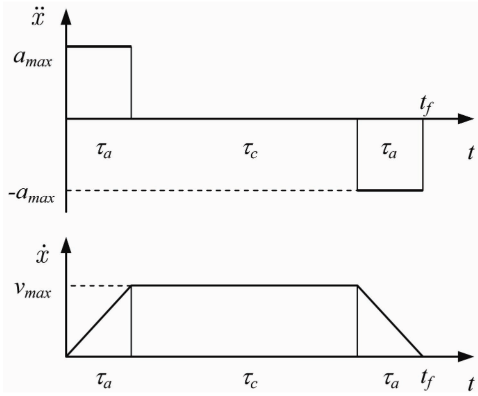

Fig. 2. Acceleration and velocity profile.

For simplicity, the accelerating phase is set to counteract the decelerating phase. Thus, motion planning is presented only in the accelerating phase.

3.1 Rectangular acceleration profile

Eq. (4) is obtained with $\ddot{x} = a = \text{const}$. Thus,

$$\theta(t) = \frac{a}{g}(\cos\omega_n t - 1), \qquad \dot{\theta}(t) = -\omega_n \frac{a}{g}\sin\omega_n t . \tag{11}$$

From Eq. (11), if the accelerating time is determined by $\tau_a = kT = 2k\pi / \omega_n$, $k = 1,2,\ldots$, multiples of the pendulum period, then $\theta(\tau_a) = 0$ and $\dot{\theta}(\tau_a) = 0$. Thus, when the constant velocity phase is switched at this time location, the swing angle is maintained at zero. The maximum velocity is determined by

$$v_{\max} = a\tau_a = \frac{2k\pi}{\omega_n} a . \tag{12}$$

Eq. (12) suggests that the integer k must be selected to ensure $a \le a_{\max}$ and the maximum swing angle may be derived from Eq. (11) as follows:

$$\theta_{\max} = \theta(\tau/2) = -\frac{2a}{g} .$$

The traveling distance is then calculated as follows:

$$\begin{aligned} p_d &= x(t_f) = v_{\max}\tau_a + \tau_c v_{\max} = v_{\max}(\tau_a + \tau_c) \\ &= a_{\max}\tau_a(\tau_a + \tau_c). \end{aligned} \tag{13}$$

where τ_c is the time of the constant velocity phase. The acceleration and velocity profiles are shown in Fig. 2.

3.2 Acceleration profile of the stair form

Based on command shaping, which has been successfully applied in control vibration systems, we use a staircase form instead of a rectangular profile to eliminate residual oscillation. Assuming that we can eliminate oscillation in the system after $N+1$ time delay, then the acceleration of the trolley is designed by

$$\ddot{x}(t)=\sum_{i=0}^{N}a_i\sigma(t-\tau_i),\ \tau_0=0,\tau_1<\tau_2<...<\tau_N \tag{14}$$

where $a_i=\text{const}$ needs to be determined, τ_N is the acceleration duration, and the step function is defined as follows:

$$\sigma(t-\tau_i)=\begin{cases}0, & t<\tau_i\\ 1, & \tau_i\le t\ .\end{cases} \tag{15}$$

Substituting Eq. (14) into Eq. (4), the following equation can be obtained:

$$\theta(t)=\frac{1}{g}\sum_{i=0}^{N}a_i\left[\cos\omega_n(t-\tau_i)-1\right]\sigma(t-\tau_i)\ . \tag{16}$$

From Eq. (16), the residual vibration in the constant velocity is given by

$$\begin{aligned}\theta(t)&=\frac{1}{g}\sum_{i=0}^{N}a_i\left[\cos\omega_n(t-\tau_i)-1\right], \qquad t\ge\tau_N\\ &=\frac{1}{g}\left\{\begin{matrix}-(a_0+a_1+...+a_N)+\\ \left(a_0\cos\omega_n\tau_0+a_1\cos\omega_n\tau_1+...+a_N\cos\omega_n\tau_N\right)\cos\omega_n t\\ +\left(a_0\sin\omega_n\tau_0+a_1\sin\omega_n\tau_1+...+a_N\sin\omega_n\tau_N\right)\sin\omega_n t\end{matrix}\right\}.\end{aligned} \tag{17}$$

Thus, the amplitude of the residual oscillation is derived from Eq. (17) by

$$V(\omega_n)=\sqrt{V_c^2+V_s^2}$$
$$\text{with } V_c=\sum_{i=0}^{N}a_i\cos\omega_n\tau_i,\ V_s=\sum_{i=0}^{N}a_i\sin\omega_n\tau_i. \tag{18}$$

Eq. (17) shows that the following constraints must be satisfied to eliminate the residual oscillation:

$$\sum_{i=0}^{N}a_i=0 \tag{19}$$

$$\sum_{i=0}^{N}a_i\cos\omega_n\tau_i=0,\quad \sum_{i=0}^{N}a_i\sin\omega_n\tau_i=0. \tag{20}$$

In addition, the trolley achieves its maximum velocity after accelerating duration τ_N. Thus,

$$\sum_{i=0}^{N-1}a_i(\tau_N-\tau_i)=v_{\max}. \tag{21}$$

Eqs. (19)-(21) form a set of four linear equations for determining the acceleration stairs of the trolley. With this acceleration profile, the residual oscillation is eliminated in the non-acceleration phases. Eqs. (19) and (20) are denoted as zero-vibration (ZV) conditions. Various cases for the number of stairs N are presented below.

Case 1. $N=1$

In this case, two unknowns need to be determined from four constraint equations

$$\begin{aligned}&a_0+a_1=0, && a_0+a_1\cos\omega_n\tau=0\\ &a_1\sin\omega_n\tau=0, && a_0\tau=v_{\max}\ .\end{aligned} \tag{22}$$

These equations can be solved when time τ is chosen such that

$$\begin{aligned}&\sin\omega_n\tau=0\ \&\ \cos\omega_n\tau=1\\ &\Rightarrow\qquad \tau=2k\pi/\omega_n,\qquad k=1,2,...\end{aligned}$$

Thus, when $\tau=2k\pi/\omega_n$, the amplitudes are given by

$$a_1=-a_0=-\frac{v_{\max}}{\tau}=-\frac{\omega_n}{2k\pi}v_{\max}\,. \tag{23}$$

The maximum swing angle is determined by

$$\begin{aligned}&\theta(t<\tau)=\frac{a_0}{g}\left[\cos\omega_n t-1\right]\\ &\Rightarrow\theta_{\max}(t=\tau/2)=-\frac{2a_0}{g}=\frac{\omega_n}{\pi g}v_{\max}\,.\end{aligned}$$

Notably, the case of $N=1$ and the case of rectangular acceleration profile are identical.

Case 2. $N=2$

From Eqs. (19) and (21), the constraints are as follows:

$$\begin{aligned}a_0+a_1+a_2&=0\\ a_0+a_1\cos\omega_n\tau_1+a_2\cos\omega_n\tau_2&=0\\ a_1\sin\omega_n\tau_1+a_2\sin\omega_n\tau_2&=0\\ a_0(\tau_2-0)+a_1(\tau_2-\tau_1)&=v_{\max}\ .\end{aligned} \tag{24}$$

Two time delays τ_1,τ_2 ($0<\tau_1<\tau_2$) should be chosen to solve Eq. (24). Choosing $\tau_1=2k\pi/\omega_n$, $\tau_2=2\tau_1$, we obtain the following:

$$\begin{aligned}&a_0+a_1+a_2=0,\\ &a_0\tau_2+a_1(\tau_2-\tau_1)=v_{\max}\,.\end{aligned}$$

These equations may be expressed in matrix form as follows:

$$\mathbf{\Phi u}=\mathbf{d},\,,$$

with

$$\mathbf{\Phi} = \begin{bmatrix} 1 & 1 & 1 \\ \tau_2 & \tau_2 - \tau_1 & 0 \end{bmatrix}, \qquad \mathbf{d} = [0, v_{\max}]^T .$$

By applying the pseudo-inverse, we obtain the solution

$$\mathbf{a} = \mathbf{\Phi}^T (\mathbf{\Phi}\mathbf{\Phi}^T)^{-1} \mathbf{d} .$$

Notably, the time τ, τ_1, τ_2 in cases $N = 1$ and $N = 2$ is chosen based on the pendulum frequency.

Case 3. $N \geq 3$

In this case, constraint Eqs. (19) and (21) are determined after choosing an arbitrary τ_i, ($i = 1, 2, ..., N$) that satisfies $0 = \tau_0 < \tau_1 < ... < \tau_N$. The time τ_N should be greater than the pendulum period of the payload; thus, $T = 2\pi / \omega_n$.

Case 4. $N \geq 5$

For $N \geq 5$, the system consisting of four constraints, that is, Eqs. (19) and (21), and $N + 1 \geq 6$ unknowns may have at least two additional equations. We set the derivative of Eq. (20) with respect to the natural frequency ω_n to zero and thus obtaining the following:

$$\begin{aligned} \frac{\partial}{\partial \omega_n} \sum_{i=0}^{N} a_i \cos \omega_n \tau_i &= \sum_{i=0}^{N} a_i \tau_i \sin \omega_n \tau_i = 0 \\ \frac{\partial}{\partial \omega_n} \sum_{i=0}^{N} a_i \sin \omega_n \tau_i &= \sum_{i=0}^{N} a_i \tau_i \cos \omega_n \tau_i = 0. \end{aligned} \tag{25}$$

Combining Eqs. (19), (21), and (25) leads to a set of six constraint equations for $N + 1 \geq 6$ unknowns. These constraint equations are denoted as zero-vibration derivative (ZVD) conditions for eliminating the residual oscillation of the payload and rewritten as follows:

$$\begin{aligned} &\sum_{i=0}^{N} a_i = 0 \\ &\sum_{i=0}^{N} a_i \cos \omega_n \tau_i = 0 \\ &\sum_{i=0}^{N} a_i \sin \omega_n \tau_i = 0 \\ &\sum_{i=0}^{N} a_i \tau_i \sin \omega_n \tau_i = 0 \\ &\sum_{i=0}^{N} a_i \tau_i \cos \omega_n \tau_i = 0 \\ &\sum_{i=0}^{N-1} a_i (\tau_N - \tau_i) = v_{\max}. \end{aligned} \tag{26}$$

3.3 Determination of time for the constant velocity phase

The constant velocity duration τ_c must be determined to ensure that the trolley reaches the desired location p_d . First, the movement distance in the accelerating phase is evaluated by integrating the velocity function from $t = 0$ to $t = \tau_N$

$$\begin{aligned} a(t) &= \sum_{i=0}^{N} a_i \sigma(t - \tau_i) \\ v(t) &= \int_0^t a(\bar{t}) d\bar{t} \\ x(\tau_N) &= \int_0^{\tau_N} v(\bar{t}) d\bar{t}. \end{aligned} \tag{27}$$

The time for constant velocity phase is then expressed as follows:

$$\tau_c = [(p_d - 2x(\tau_N))] / v_{\max} \geq 0 . \tag{28}$$

The duration τ_c must be non-negative. When this condition is not satisfied, the maximum velocity $v_{\max}$ can be reduced. Reduction of $v_{\max}$ leads to the reduction of acceleration a_i ; thus, the traveling distance in the accelerating duration $x(\tau_N)$ is also decreased.

3.4 Robustness to parameter uncertainties

The residual oscillation is eliminated with any number of stairs $N \geq 1$ when the natural frequency ω_n is precisely determined. However, this requirement may not be satisfied. In this section, the number N is selected. The dependence of the residual vibration amplitude has been assumed to be defined by Eq. (18) on ω_n and N to demonstrate the influence of the stair number N . Fig. 3 shows the magnitude $V(\omega_n, N)$ when the natural frequency of the pendulum varies around the nominal values ω_n for some cases $N = 1, 3, 5, 6$. For $N = 5$ and 6, cases including both ZV and ZVD conditions are considered. As indicated in Figs. 3(a) and (b), the magnitude of the residual vibration with $N = 1$ exhibits the highest rate of change around the location $\omega / \omega_n = 1$, and is depicted as the highest curve. The curve with $N = 3$ is lower than the curves with $N = 5$ and $N = 6$, as shown in Fig. 3(a). With the ZVD constraints considered (Fig. 3(b)), the curves with $N = 5$ (ZVD) and 6 (ZVD) are almost the same and lower than the curve with $N = 5$ (ZV) around the nominal values ω_n . Based on these figures, we

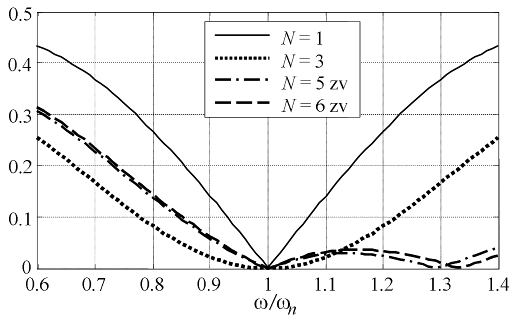

Fig. 3. Magnitude of residual vibration dependent on N and ω / ω_n .

conclude that selecting $N = 3$ for the case ZV or $N = 5$ for the case ZVD can improve the robustness of the approach.

3.5 Algorithm for determining trajectory parameters

The proposed trajectory planning method for overhead cranes can be summarized as follows:

(1) The cable length l, traveling distance or desired location p_d, and maximum velocity $v_{\max}$ are obtained.

(2) The natural frequency of the pendulum $\omega_n = \sqrt{g/l}$ and the period of vibration $T = 2\pi / \omega_n$ are calculated.

(3) The number of stairs N and time sequence are selected as follows

- Number of stairs $N = 1, 2, 3, ...$
- Time sequence:
  - If N = 1 or 2: consider $\tau_0 = 0, \tau_N = kT = k \cdot 2\pi / \omega_n$, with $k = 1, 2, ...$.
  - If N = 3, 4, … : $\tau_0 = 0$, consider freely accelerating duration $\tau_N > T = 2\pi / \omega_n$.

(4) The following are also calculated:

- Sequence of acceleration step a_i corresponding to time sequence τ_i, $i = 0, 1, ..., N$.
- Travelling distance in the accelerating and decelerating phases $d = 2 \cdot x(\tau_N)$.
- Time duration for constant velocity phase $\tau_c = [p_d - 2 \cdot x(\tau_N)] / v_{\max}$.
- Total time of operation $T_f = \tau_c + 2\tau_N = 2\tau_N + [p_d - 2 \cdot x(\tau_N)] / v_{\max}$.

4. Numerical simulations

4.1 Kinematic simulation

Numerical simulations were conducted using MATLAB to verify the validity and efficiency of the proposed approach. In the simulation, the system parameters were set as m_t = 2.0 kg, m_p = 0.85 kg, l = 1.20 m, and g = 9.81 m/s^2, and the target position of the trolley was set as x_d = 4 m. The maximum velocity is selected as $v_{\max}$ = 0.5 m/s. The pendulum frequency and the corresponding period were determined to be ω_n = 2.8592 rad/s and T = 2.1975 s. By applying the algorithm presented in Section 3, the trajectory parameters for some cases of N were obtained, as presented in Table 1.

The simulation results for the displacement and acceleration of the trolley, as well as the swing angle of the payload, are shown in Fig. 4. The desired position is achieved after a finite time. The swing angle is kept small in the non-acceleration phase and when the trolley reaches its final position. The maximum velocity can be increased without changing the acceleration duration. However, increasing maximum velocity leads to increases in the acceleration magnitude and the swing angle in the acceleration time.

To compare the robustness between the ZVD conditions and the ZV conditions, we consider the case wherein the cable length is changed to 20% of the nominal one, $l = 1.2 l_0$. The swing angles of the payload in some cases are shown in Fig. 5.

Table 1. Calculation results for some cases of N.

Case	N and k	**a** [m/s^2]	τ [s]	T_c [s]	T_f [s]	$\theta_{\max}$ [°]
1-1.	N = 1, k = 1	0.2275 −0.2275	τ = [0 2.1975]	5.802	10.197	2.654
1-2.	N = 1, k = 2	0.1138 −0.1138	τ = [0 4.3951]	3.604	12.395	1.325
2. τ_N = 1.5 T	N = 3 (ZV)	0.1138 0.1138 −0.1138 −0.1138	τ = [0 1.0988 2.1975 3.2963]	4.703	11.296	1.333
3. τ_N = 1.5 T	N = 4 (ZV)	0.0889 0.1257 −0.0000 −0.1257 −0.0889	τ = [0 0.8241 1.6482 2.4722 3.2963]	4.703	11.296	1.775
4. τ_N = 1.5 T	N = 5 (ZV)	0.0822 0.0938 0.0658 −0.0658 −0.0938 −0.0822	τ = [0 0.6593 1.3185 1.9778 2.6370 3.2963]	4.703	11.296	1.705
5. τ_N = 1.5 T	N = 5 (ZVD)	0.1107 0.0261 0.1268 −0.1268 −0.0261 −0.1107	τ = [0 0.6593 1.3185 1.9778 2.6370 3.2963]	4.703	11.296	1.420

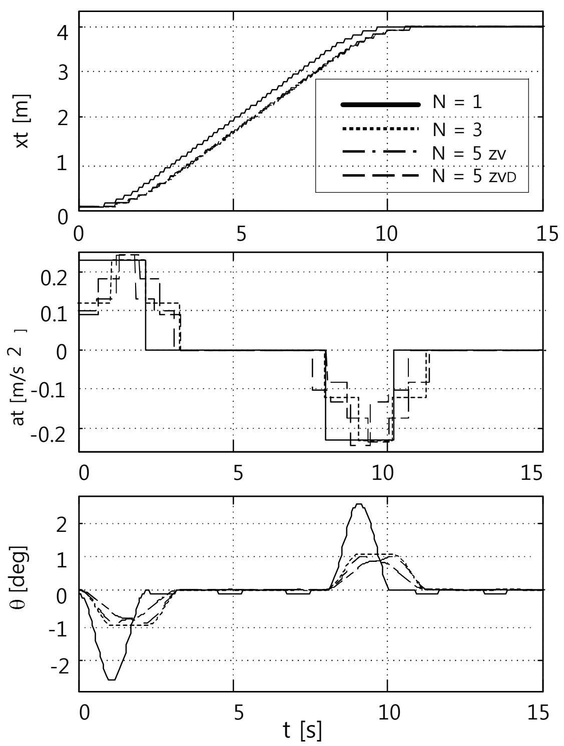

Fig. 4. Kinematic simulation results when l = 1.2 m and x_d = 4 m.

The residual oscillation of the payload when N = 5 (ZVD) is the smallest compared with other cases with N = 1 and N = 5 (ZV), as shown in Fig. 5. These results verify the robustness

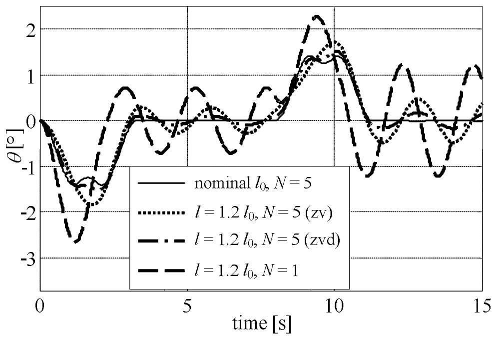

Fig. 5. Simulation results for $N = 5$ ($l = l_0$, $l = 1.2\ l_0$, ZV, and ZVD).

of the approach to the uncertainty in the cable length.

4.2 Dynamic simulation with a sliding mode controller

The trolley must be manipulated to track the designed trajectory to ensure a small swing angle in the constant velocity phase. A sliding mode controller was applied by considering disturbances induced by the payload swing. This controller was developed based on the dynamics of the trolley, and required only the trolley motion for feedback.

The control equation is given by

$$u = (m_t + m_p)\ddot{x}_r + f_{11}\dot{x} - ks - k_s \operatorname{sgn}(s) \tag{29}$$

where $\tilde{x} = x - x_d$, $\dot{\tilde{x}} = \dot{x} - \dot{x}_d$, $s = \dot{\tilde{x}} + \lambda\tilde{x}$, $\ddot{x}_r = \ddot{x}_d - \lambda\dot{\tilde{x}}$ for $\lambda > 0$, and $k > 0$, $k_s > |\delta|$ ($|\delta|$ is the uncertainty bound parameter). The control equation denoted as Eq. (29) may cause chattering in the system because of the sgn -function, and is thus replaced by a smooth function $\operatorname{sgn}(s) \approx \tanh(cs)$, with $c >> 1$.

Some simulations were performed with the controller parameters $\lambda = 2$, $k = 10$, $k_s = 2$. The simulation results for the displacement of the trolley, swing angle of the load, and control input are shown in Fig. 6. The trolley tracks the desired trajectory and reaches its destination, and the swing angle remains small. The residual oscillations in the cases $N = 3$ (ZV) and $N = 5$ (ZVD) are smaller than those in cases $N = 1$ and $N = 5$ ZV, respectively.

4.3 Experiments

Experiments with the laboratory overhead crane have been conducted to verify the proposed approach. As shown in Fig. 7, the laboratory crane used in the experiment is equipped with three direct current (DC) motors to manipulate the trolley and the bridge motions, as well as hoist the payload. Five incremental encoders with 1024 counts per revolution were used to measure the trolley and the bridge displacements, cargo-hoisting motion along the cable, and two payload swing angles corresponding to the motion directions of the trolley and the bridge. The crane system was connected to a target personal computer (PC) with two interface cards. An NI PCI-6602 card was used to send pulse-width modulation signals to the amplifiers of the DC motors and acquire signals from the encoders. An NI PCI-6025E multifunction card was used to transfer the direction control signals to the motor amplifiers. The target PC was connected to a host PC through RS-232 ports. The overhead crane was controlled by the host PC, which integrated the proposed controller design based on MATLAB/SIMULINK with xPC Target. For purpose of experiment with the proposed controller, the bridge motion and hoist motion are fixed so that the apparatus becomes two-DOF system driven only by one actuator.

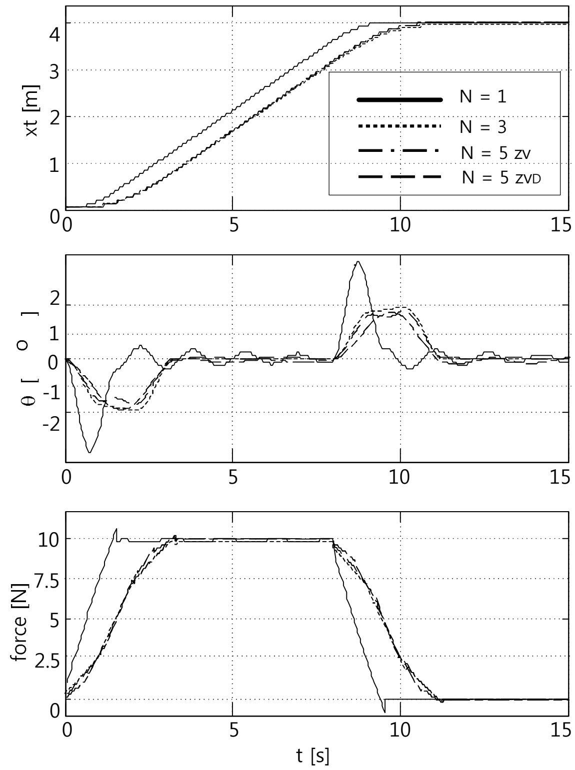

Fig. 6. Simulation results with a sliding mode controller.

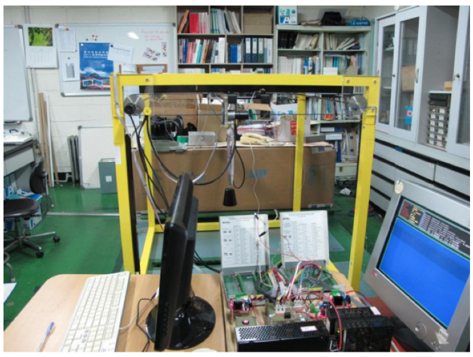

Fig. 7. Laboratory overhead crane system.

The parameters of the laboratory crane are as follows: m_t = 2.0 kg, m_p = 0.85 kg, f_{11} = 10 Ns/m, l = 0.6 m, and g = 9.81 m/s^2. The target position of the trolley is set as

$x_d = 0.5$ m. The frequency $\omega_n = 4.044$ s^{-1} of the pendulum is determined based on the cable length, and the acceleration time $\tau_N = 1.25\ T = 1.94$ s is selected. By choosing the number of stairs $N = 3$, the maximum velocity $v_{max} = 0.2$ m/s, and the time sequence $\boldsymbol{\tau} = [0\quad 0.65\quad 1.29\quad 1.94]^T$, the magnitude of stairs were determined to be $\mathbf{a} =$ $[0.083\ \ 0.061\ \ -0.061\ \ -0.083]^T$. In the previous simulation section, the system parameters were chosen to be large enough to clearly show three phases (accelerating, constant movement, and decelerating); hence, $l =$ 1.2 m and $x_d = 4$ m were set. However, in the experiment, these parameters were set to the actual values $l =$ 0.6 m and $x_d = 0.5$ m because of the limitation of the system dimension. Therefore, the acceleration and velocity profiles used in the experiment are different from those of the simulation. The obtained velocity profile of the experiment looks like a bell shape denoted as a broken line in Fig. 8. Almost no constant velocity phase exists because of such a small dimension, such that the force trajectory as control input also looks like a bell shape, as shown in Fig. 10. Meanwhile, the force trajectory of the simulation looks like a trapezoid, as shown in Fig. 6. The acceleration profile for the experiment is denoted as a broken line in Fig. 10. With the planned trajectory, the sliding mode controller of Eq. (29) is applied to the real crane system. The sliding mode controller is the same as that of the simulation and the same control parameters: $\lambda = 2$, $k = 10$, and $k_s = 2$ are applied for controlling the crane.

Similarly, for $N = 5$ (zvd) and the acceleration time $\tau_N = 1.50\ T = 2.330$ s is selected, the time sequence and the magnitude of stairs are determined as

$$\boldsymbol{\tau} = [0\quad 0.466\quad 0.932\quad 1.398\quad 1.864\quad 2.330]^T$$

$$\mathbf{a} = [0.063\quad 0.015\quad 0.072\quad -0.072\quad -0.015\quad -0.063]^T .$$

Two experiments have been carried out for N = 3 and N = 5 (zvd), in which the parameters of the controller Eq. (30) are chosen as $\lambda = 2$, $k_s = 2$, and $k = 10$.

The experimental results, including the trolley motion, swing angle, and control force, are shown in Figs. 8-10. For comparison with the numerical simulation, the responses of the simulation with $l =$ 0.6 m and $x_d = 0.5$ m are also shown as dotted lines in Figs. 8-10. The trolley reaches the target position while the swing angle is kept small at about 1° during operation for both the simulation and the experiment. Apparently, the responses of the experiment are quite similar to those of the simulation. The sway angle of the experiment is somewhat different from that of the simulation. However, considering that the maximum value of the sway is small, the difference is minimal. We assumed that the crane has only 2-dimensional motion, but the actual swing motion of the rope would be 3-dimensional in the experiment. Coupled dynamic effect of the 3D motion and un-modeled nonlinear characteristics may cause difference in swing response between the simulation and the experiment. These factors also induce residual vibration after 5 s in the experiment, as shown in Fig. 9. During the beginning of the acceleration and deceleration periods, 2-dimensional driving effect is dominant in the swing angle; hence, the experimental and simulation responses coincide. These experimental results directly confirm that a small swing angle is maintained given a suitable trajectory for the trolley. It is seen from Fig. 9 that, the swing angle for $N = 5$ is smaller than that for $N = 3$.

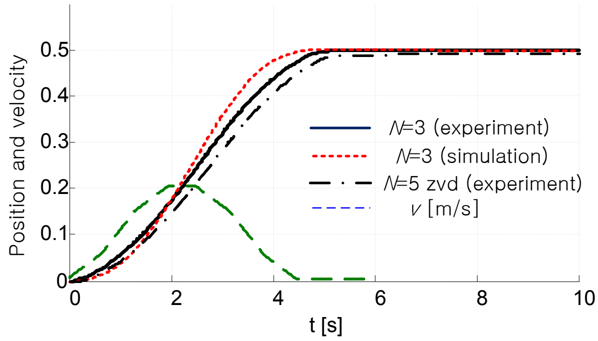

Fig. 8. Displacement and velocity of the trolley.

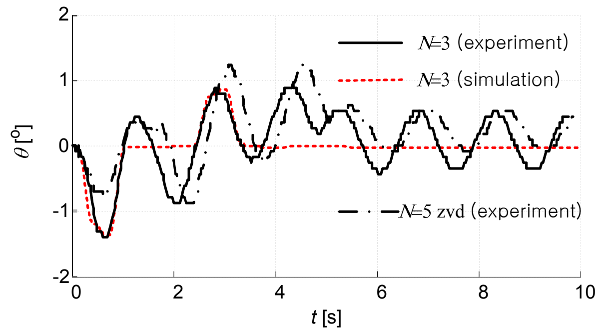

Fig. 9. Swing angle of the rope.

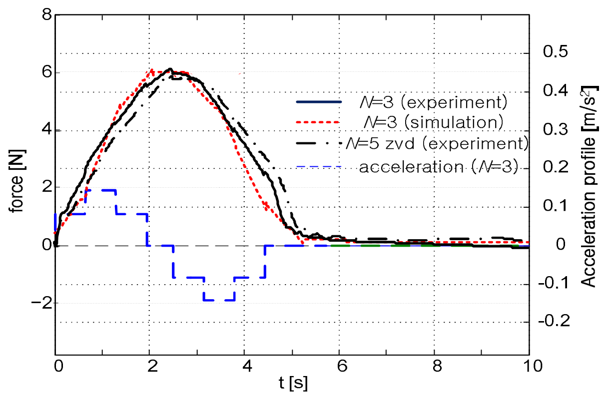

Fig. 10. Control input on the trolley.

5. Conclusions

This paper presents a simple trajectory planning method for underactuated overhead cranes using acceleration in a staircase form. This acceleration profile ensures a small swing angle of the payload during the constant velocity phase and as the trolley reaches its desired location. The efficiency of the proposed approach was verified by numerical simulation in the kinematics viewpoint and in that of crane dynamics. These simulations indicate that the payload swing is suppressed by a reasonable trajectory of the trolley and a simple controller that requires only the trolley motion for feedback. The advantages exhibited potential applications in motion planning for underactuated systems, such as overhead cranes, single-link flexible-joint manipulators, and flexible Cartesian manipulators. The proposed method intends to include three-dimensional overhead cranes in future studies.

Acknowledgment

This research was partially supported by the Ministry of Knowledge Economy (MKE) of South Korea with supervision from the Korea Evaluation Institute of Industrial Technology (KEIT) (Grant No. 10041629, Implementation of Technologies for Identification, Behavior, and Location of Human based on Sensor Network Fusion Program), the Korea Healthcare Tech-nology R&D Project, Ministry of Health and Welfare (A101987), and the Technology Innovation Program (10040992) of MKE/KEIT.

References

[1] H. M. Omara and A. H. Nayfeh, Gantry cranes gain scheduling feedback control with friction compensation, *Journal of Sound and Vibration*, 281 (2005) 1-20.

[2] D. Blackburn, W. Singhose, J. Kitchen, V. Patrangenaru, J. Lawrence, T. Kamoi and A. Taura, Command Shaping for Nonlinear Crane Dynamics, *Journal of Vibration and Control*, 16 (4) (2010) 477-501.

[3] S. Garrido, M. Abderrahim, A. Giménez, R. Diez and C. Balaguer, Anti-swinging input shaping control of an automatic construction crane, *IEEE Trans. Autom. Sci. Eng.*, 5 (3) (2008) 549-557.

[4] W. Singhose, D. Kim and M. Kenison, Input shaping control of double-pendulum bridge crane oscillations, *ASME J. Dyn. Syst. Meas. Control*, 130 (3) (2008) 1-7.

[5] B. Ma, Y. Fang and X. Zhang, Adaptive tracking control for an overhead crane system, *Proc. 17th IFAC World Congr.*, Seoul, Korea (2008) 12194-12199.

[6] H. Park, D. Chwa and K.-S. Hong, A Feedback Linearization Control of Container Cranes: Varying Rope Length, *Int. J. of Control, Automation, and Systems*, 5 (4) (2007) 379-387.

[7] L. A. Tuan, G. H. Kim, M. Y. Kim and S.-G. Lee, Partial feedback linearization control of overhead cranes with varying cable lengths, *Int. Journal of Precision Engineering and Manufacturing*, 13 (4) (2012) 501-507.

[8] L. A. Tuan, S.-G. Lee, V.-H. Dang, S.-C. Moon and B. S. Kim, Partial Feedback Linearization Control of a Three-Dimensional Overhead Crane, *International Journal of Control, Automation, and Systems*, 11 (4) (2013) 718-727.

[9] L. A. Tuan, S.-G. Lee and S.-C. Moon, Partial Feedback Linearization and Sliding Mode Techniques for 2D Crane Control, *Transactions of the Institute of Measurement and Control*, 36 (1) (2014) 78-87.

[10] N. B. Almutairi and M. Zribi, Sliding mode control of a three-dimensional overhead crane, *Journal of Vibration and Control*, 15 (11) (2009) 1679-1730.

[11] Y. Dong, Z. Wang, Z. Feng, D. Wang and H. Fang, Energy based control of a class of underactuated mechanical systems, *Congress on Image and Signal Processing*, 3 (2008) 139-143.

[12] H. H. Lee, Y. Liang and D. Segura, A sliding mode antiswing trajectory control for overhead cranes with high speed load hoisting, *Journal of Dynamic Systems, Measurements and Control*, 128 (2006) 842-845.

[13] L. A. Tuan, S.-G. Lee, H. K. Deok and L. C. Nho, Combined Control with Sliding Mode and Partial Feedback Linearization for Three-dimensional Overhead Cranes, *Int. J of Robust and Nonlinear Control* (published by online) (2013).

[14] L. A. Tuan and S.-G. Lee, Sliding mode controls of double-pendulum crane systems, *Journal of Mechanical Science and Technology*, 27 (6) (2013) 1863-1873.

[15] N. Sun and Y. Fang, New energy analytical results for the regulation of underactuated overhead cranes: an end-effector motion based approach, *IEEE Trans. on Industrial Electronics*, 59 (12) (2012) 4723-4734.

[16] N. Sun, Y. Fang, X. Zhang and Y. Yuan, Transportation task-oriented trajectory planning for underactuated overhead cranes using geometric analysis, *IET Control Theory Appl.*, 6 (4) (2012) 1410-1423.

[17] Y. J. Hua and Y. K. Shine, Adaptive coupling control for overhead crane systems, *Mechatronics*, 17 (2007) 143-152.

[18] L. A. Tuan, S.-G. Lee, L. C. Nho and D.-H. Kim, Model reference adaptive sliding mode control for three dimensional overhead cranes, *International Journal of Precision Engineering and Manufacturing*, 14 (8) (2013) 1329-1338.

[19] C. Chang, Adaptive fuzzy controller of the overhead cranes with nonlinear disturbance, *IEEE Trans. Industrial Informatics*, 3 (2) (2007) 164-172.

[20] D. Liu, J. Yi, D. Zhao and W. Wang, Adaptive sliding mode fuzzy control for a two-dimensional overhead crane, *Mechatronics*, 15 (5) (2005) 505-522.

[21] L. A. Tuan, S.-C. Moon., W. G. Lee and S.-G. Lee, Adaptive sliding mode control of the overhead crane with varying cable length, *Journal of Mechanical Science and Technology*, 27 (3) (2013) 885-893.

[22] Q. H. Ngo and K.-S. Hong, Adaptive sliding mode control of container cranes, *IET Control Theory Appl.*, 6 (5) (2012) 662-668.

[23] Q. H. Ngo and K.-S. Hong, Sliding-mode antisway control of an offshore container crane, IEEE/ASME *Trans. Mechatron.*, 17 (2) (2012) 201-209.

[24] M. S. Park, D. Chwa and S. K. Hong, Antisway tracking

control of overhead cranes with system uncertainty and actuator nonlinearity using an adaptive fuzzy sliding-mode control, *IEEE Trans. Industrial Electronics*, 55 (11) (2008) 3972-3984.

[25] Y. Fang, W. E. Dixon, D. M. Dawson and E. Zergeroglu, Nonlinear coupling control laws for an underactuated overhead crane system, *IEEE/ASME Transactions on Mechatronics*, 8 (3) (2003) 418-423.

[26] H. Aschemann, Passivity-based trajectory control of an overhead crane by interconnection and damping assignment, *Motion and Vibration Control*, Springer (2009) 21-30.

[27] H.-H. Lee, A new motion-planning scheme for overhead cranes with high-speed hoisting, *Journal of Dynamic Systems, Measurement and Control*, 126 (2004) 359-364.

[28] H.-H. Lee, Motion planning for three-dimensional overhead cranes with high-speed load hoisting, *International Journal of Control*, 78 (12) (2005) 875-886.

[29] M. W. Spong, S. Hutchinson and M. Vidyasagar, *Robot dynamics and control*, John Wiley & Sons (2005).

Nguyen-Quang Hoang received his B.E. and M.S. degrees in Applied Mechanics from Hanoi University of Science and Technology (HUST), Hanoi, Vietnam; and his Ph.D. in Mechanical Engineering from the Hamburg University of Technology, Germany, in 1997, 1999 and 2006, respectively. Since 2006, he works as lecturer at the Department of Applied Mechanics, School of Mechanical Engineering of HUST, Hanoi, Vietnam. From 9/2012 to 9/2013 he received an Postdoctoral Fellowship at the Department of Mechanical Engineering of Kyung Hee University, Yongin, Korea. His research interests include engineering vibration, modelling and control of dynamic systems, dynamics of multibody systems, and numerical simulation.

Soon-Geul Lee received his B.E. degree in Mechanical Engineering from Seoul National University, Seoul, Korea; his M.S. in Production Engineering from KAIST, Seoul, Korea; and his Ph.D. degree in Mechanical Engineering from the University of Michigan in 1983, 1985 and 1993, respectively. Since 1996, he has been with the Department of Mechanical Engineering of Kyung Hee University, Yongin, Korea, where he is currently a Professor. His research interests include robotics and automation, mechatronics, intelligent control, and biomechanics. He likewise served as the Director of the Korean Society of Precision Engineering (KSPE) (2005-2007) and for the Institute of Control, Automation, and Systems Engineers (ICASE) (2006).

Hyung Kim received his B.E. degree in Mechanical Engineering from Korean Educational Development Institute, his M.S. degree in Mechanical Engineering from KyungHee University, Korea. He got trained from the Korea Institute of Industrial Technology, Korea as researcher. He is currently pursuing a Ph.D. at the Kyung Hee University. His research interests are in the area of Autonomous Mobile robot, Intelligent robot.

Sang-Chan Moon received the B.C. and M.S. degrees in Department of Mechanical Engineering from Kyung Hee University. Since 2012, he is currently pursuing a Ph.D. degree at the Department of Mechanical Engineering, Kyung Hee University. His research interests are in the area of developing a precision positioning system using GPS based on v2x networks for intelligent vehicle or mobile robot.